Regularized 13-Moment-Equations

Manuel Torrilhon

*Applied Mathematics, Princeton University, USA, email:*mtorrilh@princeton.edu

Abstract. In this paper we present fundamental properties and new results for the regularized 13-moment-equations. These equations form a new continuum model for rarefied gas flow with Knudsen number $Kn < 1$. Stability results and shock profile performance is reviewed and testing results for light scattering are presented. Questions of hyperbolicity and two-dimensional flow simulations are discussed.

Keywords: kinetic gas theory, transport theory, regularized 13-moment-equations
PACS: 51.10

INTRODUCTION

One problem in kinetic gas theory is to find continuum models that accurately approximate Boltzmann's equation as partial differential equations in space-time only [12]. The aim is to find a compact system of field equations for fluid variables that describe processes up to moderate values of the Knudsen number reaching beyond the range where ordinary fluid dynamics of Navier-Stokes and Fourier (NSF) is applicable. Classical approaches are the Chapman-Enskog expansion that yields Burnett and super-Burnett equations, or Grad's moment method that provides ever larger systems of equations.

Only recently, new equations were presented in [14], named regularized 13-moment-equations (R13). They are derived by means of a Chapman-Enskog expansion around a non-equilibrium given by Grad's distribution function. This approach provides a general constitutive theory for regularization of moment equations obtained in Grad's theory as in [4], [6]. The regularization introduces gradient terms into the fluxes of the moment equations and produces parabolic-hyperbolic partial differential equations. These additional terms are of higher order in the Knudsen number and both stabilize the system and improve its physical accuracy considerably.

Several earlier paper are related in spirit to the R13 derivation. In [9] a hybrid Chapman-Enskog approach was explored by looking at the defect of the kinetic equation for a specified distribution function, like Grad's distribution. The result are linearized equations with unknown coefficients exhibiting a similar structure as the R13 equations. The authors of [7] tried to regularize Burnett equations by transforming it into a hyperbolic relaxation system in an ad hoc way. Again, the structure of their equations is similar to the R13 system, but exhibits clear deviations from the general structure of transfer equations. In [10] a possbile parabolization of moment equations is discussed.

The R13 equations succeeds over all these approaches by providing a fully three-dimensional non-linear system following rigerously from Boltzmann's equation. The basic features are

- accuracy up to third order in Knudsen number in an asymptotic expansion,
- fully stable for all frequencies and wave numbers,
- smooth shock profiles for large Mach numbers,
- compact second order field equations, convenient for numerical and analytical purposes.

This paper reviews basic results for the R13 system, like stability and smooth shock profiles. New results include the discussion of hyperbolicity and the testing by light scattering experiments. The paper also shows two-dimensional simulation results.

R13 EQUATIONS

Here we only present the final equations of the R13 system, for a detailed derivation see [14].

The set of variables in the R13 equations is given by density ρ, velocity v_i, temperature θ (in energy units), pressure deviator σ_{ij} (called stress for simplicity) and heat flux q_i. The necessary constitutive relations for stress and heat flux

are given by the transfer equations

$$\begin{aligned}
\partial_t \sigma_{ij} + \partial_k(\sigma_{ij} v_k) + \tfrac{4}{5}\partial_{\langle i} q_{j\rangle} + 2p\partial_{\langle i} v_{j\rangle} + 2(\partial_k v_{\langle i})\sigma_{j\rangle k} + \partial_k m_{ijk} &= -\tfrac{\mu}{p}\sigma_{ij} \\
\partial_t q_i + \partial_k(q_i v_k) + p\,\partial_k(\sigma_{ik}/\rho) + \tfrac{5}{2}p\,\partial_i\theta + \tfrac{5}{2}\sigma_{ik}\partial_k\theta - \tfrac{\sigma_{ij}}{\rho}\partial_k\sigma_{jk} & \\
+\tfrac{7}{5}q_k\partial_k v_i + \tfrac{2}{5}q_k\partial_i v_k + \tfrac{2}{5}q_i\partial_k v_k + \tfrac{1}{2}\partial_k\hat{R}_{ik} + m_{ijk}\partial_j v_k &= -\tfrac{2}{3}\tfrac{\mu}{p}q_i
\end{aligned} \tag{1}$$

following from Boltzmann's equation. Here, $p = \rho\theta$ is the pressure and μ is the viscosity of the gas. The productions are obtained for the case of Maxwell molecules, but extrapolated to general molecules by the use of general expressions of μ. If the higher moment contributions $\hat{R}_{ij}$ and m_{ijk} are set to zero in (1) the equations turn into the classical Grad 13-moment-case. The new regularization procedure of [14], however, provides the expressions

$$\begin{aligned}
m_{ijk} &= -2\mu\,\partial_{\langle k}(\sigma_{ij\rangle}/\rho) + \tfrac{8}{10p}q_{\langle i}\sigma^{(\mathrm{NSF})}_{jk\rangle} + m^{(2)}_{ijk}\,, \\
R_{ij} &= -\tfrac{24}{5}\mu\,\partial_{\langle i}(q_{j\rangle}/\rho) + \tfrac{32}{25p}q_{\langle i}q^{(\mathrm{NSF})}_{j\rangle} + \tfrac{24}{7\rho}\sigma_{k\langle i}\sigma^{(\mathrm{NSF})}_{j\rangle k} + R^{(2)}_{\langle ij\rangle}\,, \\
R &= -12\mu\,\partial_k(q_k/\rho) + \tfrac{8}{p}q_k q^{(\mathrm{NSF})}_k + \tfrac{6}{\rho}\sigma_{ij}\sigma^{(\mathrm{NSF})}_{ij} + \tfrac{5}{2}R^{(2)}_{kk}\,.
\end{aligned} \tag{2}$$

with $\hat{R}_{ij} = R_{ij} + \frac{1}{3}R\delta_{ij}$ and the abbreviations

$$\sigma^{(\mathrm{NSF})}_{ij} = -2\mu\,\partial_{\langle i} v_{j\rangle}, \qquad q^{(\mathrm{NSF})}_i = -\tfrac{15}{4}\mu\,\partial_i\theta, \tag{3}$$

$$m^{(2)}_{ijk} = \tfrac{2\mu}{\rho p}(\partial_l\sigma_{l\langle i})\sigma_{jk\rangle}, \quad R^{(2)}_{ij} = \tfrac{4\mu}{\rho p}(\sigma_{ij}\partial_k q_k + \sigma_{ij}\sigma_{kl}\partial_l v_k + \tfrac{6}{5}(\partial_k\sigma_{ki})q_j). \tag{4}$$

Note the special structure in (2): The leading expression is a gradient term that produces a Laplacian of stress and heat flux in their respective equation in (1). This is similar to the Navier-Stokes-Fourier system which can be viewed as regularization of the Euler equations. The next terms in (2) are products of the stress and heat flux and their NSF counterpart. The last expressions $m^{(2)}_{ijk}$ and $R^{(2)}_{ij}$ form terms of higher order in the Knudsen number, see [13].

The R13 equations are given by the general conservation laws plus the evolution equations (1) closed with the expressions (2).

Accuracy and Stability

We define the *Knudsen order* as a theoretical accuracy measure in the following way: Stress and heat flux can be expanded in terms of Knudsen number based on the R13 system alone. This expansion will differ from the expansion based on the full Boltzmann equation. If the leading exponent of the Knudsen number in the difference of both expansions is $n+1$, the Knudsen order of the system will be n. According to this definition the Euler equations have Knudsen order $n = 0$, while the NSF system has $n = 1$. A large Knudsen order is expected to provide high physical accuracy.

In [14] and [17] detailed expansions have been conducted for the R13 equations. The results show that the R13 system has a Knudsen order of $n = 3$,which is the same order as super-Burnett equations. It is well known that Burnett and super-Burnett equations following from the direct expansion of the Boltzmann equation are inherently unstable equations, see [2]. In [14], however, it is proven that the R13 system does not share this deficiency. A linear stability shows that R13 is fully stable both for temporal and spatial modes, see Fig. 1.

With these results the R13 system is the most accurate and stable continuum model currently available.

Smooth Shock Profiles

The classical 13-moment-case of Grad produces sub-shocks in shock wave profiles for Mach numbers $M_0 > 1.65$. Hence, Grad's 13-moment-case is essentially useless for calculations involving shocks. The new regularized equation overcome this deficiency and produce smooth shock profiles also for high Mach numbers.

The left hand side of Fig. 2 shows a shock wave profile calculated with R13 for Maxwell molecules at $M_0 = 3.0$. The plot shows the normalized profiles of density and heat flux and the smoothness is clearly visible. The dots mark the

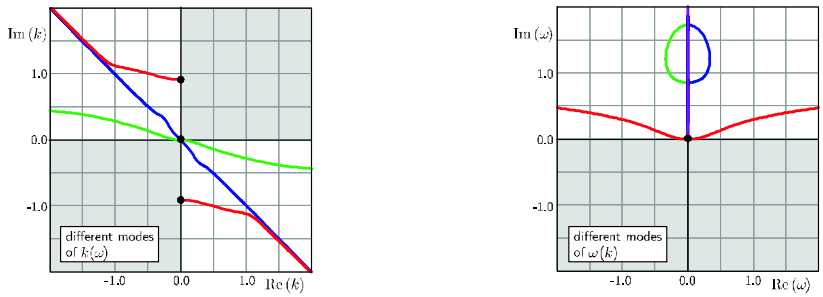

FIGURE 1. Linear stability analysis for regularized 13-moment-equations. Left: spatial modes. Right: temporal modes. Grey shading marks unstable regions. All R13 modes are fully stable.

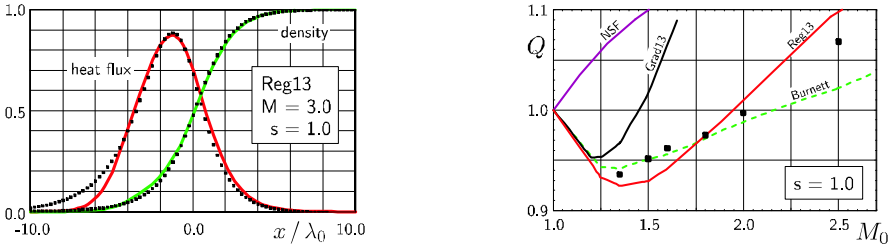

FIGURE 2. Left: normalized density and heat flux in shock profile at $M_0 = 3.0$ by R13 equations for Maxwell molecules. Right: shock asymmetry over Mach number for various models. Dots are DSMC results.

results of a DSMC calculation. The agreement is good and becomes better for smaller Mach numbers. The deviations especially in the upstream area become more pronounced for higher Mach numbers. For Mach numbers $M > 4$ the regularized 13-moment-equations deviates strongly from the DSMC result and applicability of the theories is no longer given, if quantitative features are needed to be captured. For more details on the performance of R13 for shock waves, see [17].

The shock asymmetry gives information about the actual shape of the profile condensed in a single number. Its value is much more difficult to match by continuum models than the shock thickness. The asymmetry is defined as $Q = \int_{-\infty}^{x^\star} (\rho(x) - \rho_0)\, dx \,/\, \int_{x^\star}^{\infty} (\rho_1 - \rho(x))\, dx$ where the position $x^\star$ is determined by the relation $\rho(x^\star) = \frac{1}{2}(\rho_0 + \rho_1)$.

In the right hand side of Fig. 2 shock asymmetry results obtained by DSMC simulations are presented together with the theoretical curves of the NSF theory, Grad's 13-moment-case, the Burnett model and the R13 system. All results are for Maxwell molecules with viscosity exponent $s = 1$. The results of NSF indicate a qualitative failure. The curve predict an asymmetry $Q > 1$ from the very beginning (i.e. already for small Mach numbers), which is in clear contradiction not only to DSMC simulations but also to measurements, see e.g. [1]. The asymmetry results of the classical 13-moment-system of Grad lie far off. The Burnett results are acceptable, however, they are based on unstable equations requiring low grid sizes. The R13 solution matches the DSMC results in a reasonable manner.

Hyperbolicity

Formally, the R13 expressions (2) are made from gradients which enter the divergences in the transfer equations (1). Hence, the mathematical structure of the R13 equations is given by the classical, hyperbolic Grad equations enriched by a parabolic expression in the form $\mathrm{div}\,(D(\mathbf{U}) \cdot \mathrm{grad}\,\mathbf{U})$, where $\mathbf{U}$ are the variables and D some coefficients. In this way the hyperbolic base given by Grad's 13-moment-case remains unchanged. However, variants of the derivation of the R13 system, see [13], indicate that in some of the product terms in (2) the NSF expression can be replaced by the variable itself, $\sigma_{ij}^{(NSF)} \to \sigma_{ij}$ and $q_i^{(NSF)} \to q_i$. Note, that this does not change the Knudsen order and the formal accuracy of the system, since the replacement only introduces terms of higher order in the Knudsen number. But the new terms are purely algeraic and influence the hyperbolic behavior of the underlying Grad flux in (1).

Fig. 3 investigates the possible effect on the domain of hyperbolicity. The classical 13-moment-case of Grad exhibits

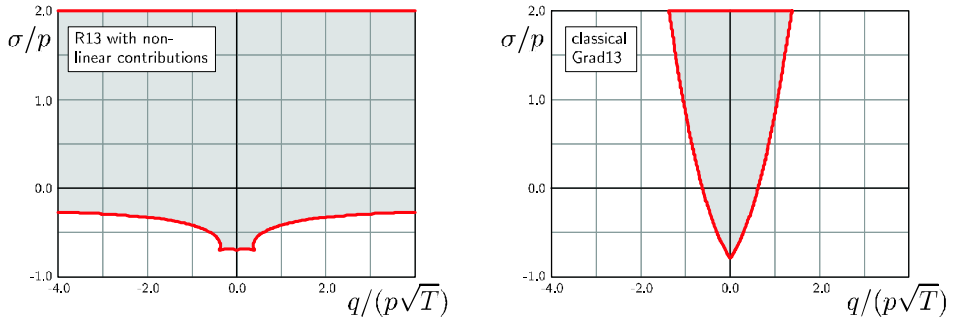

FIGURE 3. Hyperbolicity region for classical 13-moment-case by Grad (right) and the R13 equations with non-linear regularization (left).

hyperbolicity only in a small vicinity of the equilibrium state. The hyperbolicity depends on the one-dimensional values of normal stress and heat flux in dimensionless form and its boundary is ploted on the right hand side of Fig. 3. This lack of hyperbolicity is investigated in [8], [11], and [15]. Interestingly, the non-linear contributions from the R13 relations open the domain of hyperbolicity considerably, see left hand side of Fig. 3. Note, that due to the definition of the pressure deviator we have $-1 < \sigma/p < 2$. The positive effect could be attributed to the regularizing character of the R13 expressions viewed in the hyperbolic setting. These findings require additional investigations and are subject of ongoing work.

LIGHT SCATTERING RESULTS

In light scattering experiments in gases density fluctuations result in the scattering of a laser beam. The spectral density, given by the spatial and temporal Fourier transform of the auto-correlated electric field of the scattered light, can be measured by a Fabry-Perot interferometer. It is given by

$$S(\hat{q},\hat{\omega}) = \frac{1}{2\pi}\int_{-\infty}^{\infty} \left\langle E^{(s)}(\hat{q},0)\, E^{(s)}(\hat{q},\tau)\right\rangle e^{i\,\hat{\omega}\,\tau}\, d\tau \tag{5}$$

where $E^{(s)}$ is the scattered electric field and $\langle . \rangle$ denote the auto-correlation. The scattered electric field is proportional to the fluctuations of the density $E^{(s)}(\hat{q},\tau) \sim \delta\rho(\hat{q},\tau)$. The dimensionless frequency of the scattered light is denoted by $\hat{\omega}$ and $\hat{q}$ is its dimensionless wave length, which corresponds to the spatial wave length of the density fluctuation. Based on the Onsager hypothesis, the auto-correlation of the density fluctuation can be computed by averaging the solutions of the linearized macroscopic field equations. The challenge is to correctly predict the measured function $S(\hat{q},\hat{\omega})$ with the macroscopic equations. For more details about the measurement and computation of light scattering, please see Chapter 10 in [11] or the review [18].

Small values of $\hat{q}$ represent large scale fluctuations. On the other hand, ever larger values of $\hat{q}$ indicate small fluctuations, eventually of the same order as the mean free path. Indeed, in the dimensionless setting we have $\hat{q} \approx Kn$. It becomes clear, that predicting light scattering experiments with large values of $\hat{q}$ will be difficult for classical fluid equations.

Measurements [3] of the spectral density are shown in Fig. 4 for the case $\hat{q} = 1$ as dots. The function $S(\hat{q} = 1, \hat{\omega})$ shows a central peak (Rayleigh peak) and two symmetric peaks to each side (Brillouin peaks). The central peak appears at the value of the incoming frequency (shifted to zero in the plots) and represents the diffusion mode of the fluctuation. The two Brillouin peaks represent sound modes and are locted where ω/q equals approximately the sound speed.

The left hand side of Fig. 4 shows the theoretical results for $S(\hat{q} = 1, \hat{\omega})$ for the NSF system, Grad's 13-moment-case and Burnett equations. None of these models succeed in matching the measurements. Only for smaller values of $\hat{q}$ the peaks become more pronounced and all the models occasionally match the experiment (not shown). However, $\hat{q} = 1$ captures such small fluctuations that the respective models fail. Note, that Grad's equations do not even produce three peaks. The right hand side of Fig. 4 shows the theoretical result for the regularized 13-moment-equations. It is clearly superior over all classical models.

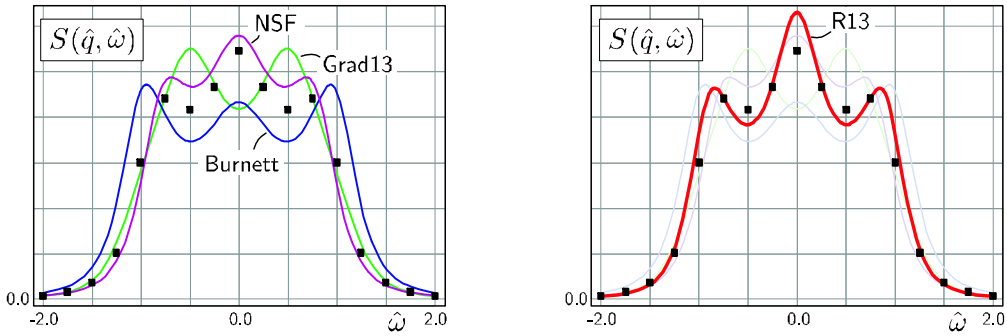

FIGURE 4. Light scattering: Spectral density $S(\hat{q},\hat{\omega})$ at angle $\hat{q} = 1.0$ for classical models (left) and R13 equations (right). Dots are measurements.

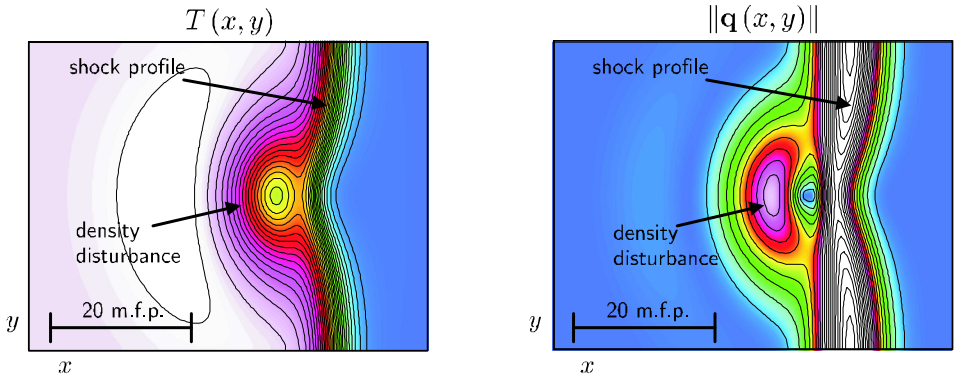

FIGURE 5. Two-dimensional flow: a shock wave with $M_0 = 2.0$ interacts with a micro disturbance, temperature field (left) and amplitude of heat flux (right). Initially, the disturbance has a density ratio of 2 and constant pressure.

TWO-DIMENSIONAL FLOW

This section presents some two-dimensional flow solutions for the R13 system. A specific flow situation is chosen in which a shock wave interacts with a dense micro-disturbance. The example demonstrates the performance of the R13 equations for two-dimensional bulk flows in absence of boundaries. The simulation is conducted for decreasing disturbance diameter d from $d = 20\lambda_0$ to $d = 10\lambda_0$ where λ_0 is the mean free path. The results are compared to Navier-Stokes-Fourier.

In the initial conditions a shock wave profile is situated with its density barycenter at $x = -1.0$ traveling in positive x-direction with Mach number $M_0 = 2.0$ into a flow field at rest with $(\rho, \theta, p) = (1, 1, 1)$. Around $(x, y) = (0.5, 0.0)$ a circular density disturbance is placed with a Gaussian density distribution of height 1.5 and diameter $d = 1$ and constant pressure. Due to constant pressure the interior of the disturbance will be colder than the environment. The entire computational domain is given by $[-2, 3] \times [-1, 1]$. The numerical method is described in [16].

The simulations will be based on dimensionless R13 equations (1)/(2) for Maxwell molecules ($\mu \sim \theta$) in which only the Knudsen number remains to be specified. We choose $Kn = 0.05, 0.1$, hence, the distance $\Delta x = 1$ corresponds to 20 and 10 mean free paths of the reference state, respectively. Accordingly, the diameter of the density bump will decrease its actual physical range. However, the shock wave profile will be initialized in agreement with the Knudsen number. This leads to a broader or thinner numerical profile.

To give an impression of the distortion of the shock front due to the density disturbance Fig. 5 shows contour plots of temperature and amplitude of the heat flux at time $t = 0.8$. The result shown is based on $Kn = 0.05$ and the range $x \in [0, 2] \times [-1, 1]$. At the time shown in the figure the front has just passed through the disturbance. The bump is now placed behind the shock. The temperature front is dented due to the interaction. A strong kink is also visible in the soliton shaped heat flux which interacts with the heat flux inside the bump. All other fields like density and stress exhibit corresponding behavior.

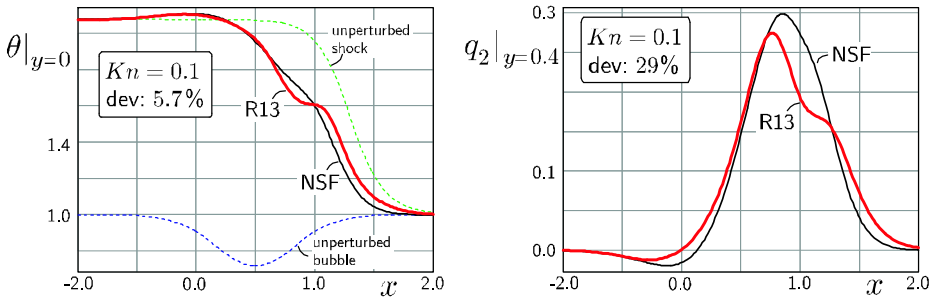

FIGURE 6. Comparison with Navier-Stokes-Fourier in the case of the shock interaction with a micro disturbance. The more accurate R13 model shows strong deviations for this bulk flow example.

We will now compare the solutions of the R13 system and the NSF equations for this simulation. Any difference must be related to the first order character of the constitutive relations of NSF which becomes most pronounced for larger Knudsen numbers. Due to the higher kinetic accuracy of the R13 system we expect its solution to be the physically relevant one.

At time $t = 0.8$ the shock front is just about to exit the bump. This situation shows the strongest non-equilibrium and correspondingly the strongest differences between the models. One-dimensional cuts for temperature θ and heat flux component q_2 in the case $Kn = 0.1$ are shown in Fig. 6. Temperature is shown along the center line $y = 0$, while q_y follows a line 4 mean free path off the center. The dashed lines in the temperature plots give a reference to the unperturbed fields of the shock front and density bump, respectively. The solution of the NSF system is shown using thin lines. The plots show a clear difference between the models. At this scale the bump has an initial diameter of ten mean free paths. The solution of the R13 system is less smeared out showing shoulders in the profiles. The NSF solution is smoother indicating a faster relaxation due to less inertia. The smeared out temperature field of NSF solution leads to a mismatch in the actual shock position. The failure of Navier-Stokes-Fourier is also manifested in almost 30% deviation in the heat flux.

We note that the differences originate purely from the lack of accurate high order non-equilibrium multi-scale modeling in the simple NSF system. In that sense the deviations are a bulk effects and can obviously not be influenced by boundary conditions like slip models. For more details, see [16].

REFERENCES

1. Alsmeyer, H., *J. Fluid Mech.* **74**(3), pp.497-523, (1976).
2. Bobylev, A. V., *Sov. Phys. Dokl.* **27**, pp.29-31, (1982).
3. Clark, N. A., *Ineleastic light scattering from thermal fluctuations in gases*, PhD thesis, MIT, 1970.
4. Grad, H., *Comm. Pure Appl. Math.* **2**, pp.331-407, (1949).
5. Grad, H., *Comm. Pure Appl. Math.* **5**, pp.257-300, (1952).
6. Grad, H., "Principles of the Kinetic Theory of Gases", in *Handbuch der Physik*, vol.12, edited by S. Flügge, Springer, Berlin, 1958.
7. Jin, S. and Slemrod, M., *J. Stat. Phys.* **103**(5-6), pp.1009-1033, (2001)
8. Junk, M., *J. Stat. Phys.* **93**(5-6), pp.1143-1167, (1998).
9. Karlin, I. V., Gorban, A. N., Dukek, G., and Nonnenmacher, T. F., *Phys. Rev. E* **57**(2), pp.1668-1672, (1998) .
10. Müller, I., Reitebuch, D., and Weiss, W., *Cont. Mech. Therm.*, **15**(2), pp.411-425, (2002).
11. Müller, I., and Ruggeri, T., *Rational Extended Thermodynamics* (2nd edn), Springer Tracts in Natural Philosophy (vol.37), Springer, NewYork, 1998.
12. Struchtrup, H., *Macroscopic Transport Equations for Rarefied Gas Flows*, Interaction of Mechanics and Mathematics, Springer, New York, 2005.
13. Struchtrup, H., *Phys. Fluids* **16**(11), pp.3921-3934, (2004).
14. Struchtrup, H. and Torrilhon, M., *Phys. Fluids* **15**/9, pp.2668-2680, (2003).
15. Torrilhon, M., *Cont. Mech. Therm.* **12**/5, pp. 289-295, (2000).
16. Torrilhon, M., *Multiscale Model. Simul.*, in press, (2006).
17. Torrilhon, M. and Struchtrup, H., *J. Fluid Mech.* **513**, pp.171-198, (2004).
18. Weiss, W. and Müller, I., *Cont. Mech. Therm.* **7**(2), pp. 123-177 (1995).